Biomacromolecules

pubs.acs.org/Biomac

Article

UV-Triggered On-Demand Temperature-Responsive Reversible and Irreversible Gelation of Cellulose Nanocrystals

Christoph Hörenz, Kia Bertula, Tony Tiainen, Sami Hietala, Ville Hynninen, and Olli Ikkala*

Cite This: *Biomacromolecules* 2020, 21, 830–838

Read Online

ACCESS | Metrics & More | Article Recommendations | Supporting Information

ABSTRACT: We show ionically cross-linked, temperature-responsive reversible or irreversible hydrogels of anionic cellulose nanocrystals (CNCs) and methacrylate terpolymers by mixing them homogeneously in the initially charge-neutral state of the polymer, which was subsequently switched to be cationic by cleaving side groups by UV irradiation. The polymer is a random terpolymer poly(di(ethylene glycol) methyl ether methacrylate)-*rnd*-poly(oligo(ethylene glycol) methyl ether methacrylate)-*rnd*-poly(2-((2-nitrobenzyl)oxycarbonyl)aminoethyl methacrylate), that is, PDEGMA-*rnd*-POEGMA-*rnd*-PNBOCAEMA. The PDEGMA and POEGMA repeating units lead to a lower critical solution temperature (LCST) behavior. Initially, homogeneous aqueous mixtures are obtained with CNCs, and no gelation is observed even upon heating to 60 °C. However, upon UV irradiation, the NBOCAEMAs are transformed to cationic 2-aminoethyl methacrylate (AEMA) groups, as 2-nitrobenzaldehyde moieties are cleaved. The resulting mixtures of anionic CNC and cationic PDEGMA-*rnd*-POEGMA-*rnd*-PAEMA show gelation for sufficiently high polymer fractions upon heating to 60 °C due to the interplay of ionic interactions and LCST. For short heating times, the gelation is thermoreversible, whereas for long enough heating times, irreversible gels can be obtained, indicating importance of kinetic aspects. The ionic nature of the cross-linking is directly shown by adding NaCl, which leads to gel melting. In conclusion, the optical triggering of the polymer ionic interactions in combination with its LCST phase behavior allows a new way for ionic nanocellulose hydrogel assemblies.

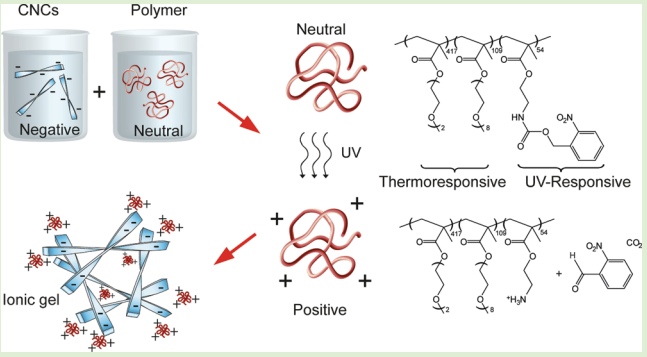

1. INTRODUCTION

Nanocelluloses are colloidal fibrils that can be cleaved from plant or wood resources or produced bacterially.[1] They have been actively pursued recently due to their sustainable origin; good mechanical properties; potential to allow functionalization in a wide range to make composite materials, gels, aerogels, fibers, biochemical scaffolds, films, coatings, viscosity modifiers, and structural colors; and biocompatibility.[2] The good mechanical properties of native nanocelluloses arise from their internal hydrogen-bonded structures of the constituent parallel-aligned cellulose chains. Nanocelluloses include cellulose nanofibers (CNF), cellulose nanocrystals (CNC), tunicates, and bacterial celluloses (BC), each having nanoscopic lateral dimensions and lengths depending on the type. In particular, CNCs are rod-like with lateral dimensions of approximately 5−15 nm and lengths from tens to hundreds of nanometers, depending on the processing conditions and sources.[3]

On the other hand, as hydrogels are important in many fields of science and technology,[4] nanocellulose-based hydrogels have also been extensively pursued. Therein, the higher aspect ratio CNFs inherently form gels,[5,6] whereas the shorter aspect ratio rod-like nanocelluloses require additional components or cross-linking engineering steps to form the network connectivity for gelation.[7−35]

As the CNCs typically are negatively charged due to their sulfate ester groups arising from the sulfuric acid hydrolysis, one could ask whether CNC-based hydrogels could be fabricated by simply using ionic interactions as the network cross-links upon mixing the anionic CNCs with cationic polymers within the aqueous medium. In the state of the art, well-defined ionic self-assemblies have been achieved, taken that the matching ionic interactions do not lead to cross-linkings, that is, there is only one oppositely charged site in the interacting molecules.[36] There are, however, potential problems to be expected if several charged sites are encountered in each component, as simply mixing the negative and positive components in their aqueous solutions may lead to uncontrolled and nonuniform aggregations, as the electrostatic interactions are of long range. Therefore, a classic approach in interpolyelectrolyte complexation between the

Received: November 5, 2019
Revised: January 15, 2020
Published: January 15, 2020

https://dx.doi.org/10.1021/acs.biomac.9b01519
Biomacromolecules 2020, 21, 830−838

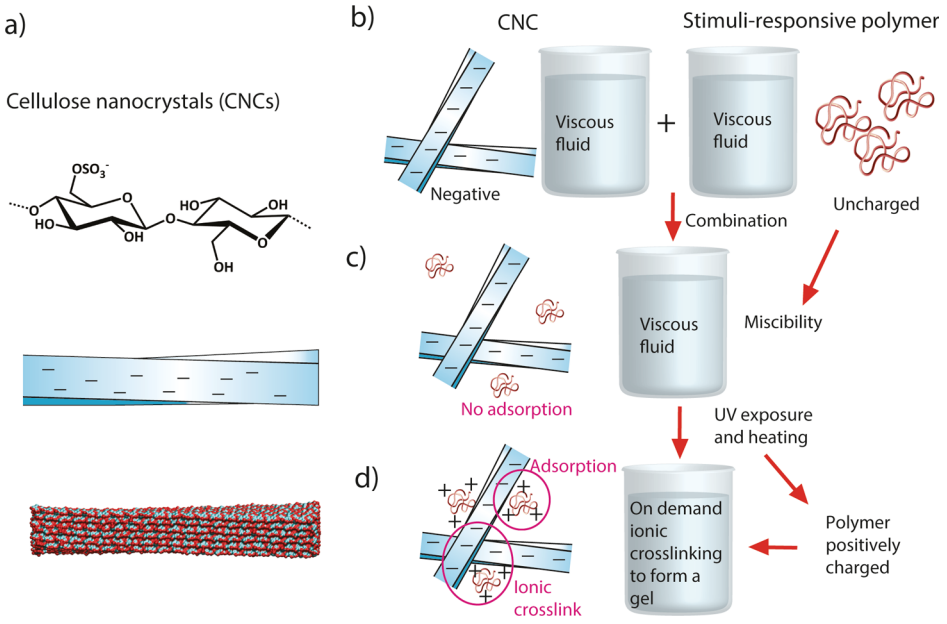

Figure 1. Suggested generic scheme to achieve homogeneous aqueous mixtures of (a) the negatively charged CNCs and (b) positively charged polymers using an initially neutral polymeric precursor and (c) using a UV-triggerable cationization thereof to form (d) ionic cross-linkings on-demand between CNCs, resulting in gel networks also driven by an additional LCST-functionalization of the polymer. The CNC model in panel (a) is adapted with permission from ref 50. Copyright 2013 American Chemical Society.

anionic and cationic components is a controlled screening of the ionic interactions upon adding salts or tuning the pH.[37−42]

On the other hand, various routes for photoinduced and phototriggerable hydrogelations have been reported.[43−48] In the present work, a question can be posed whether a homogeneous aqueous mixture could be achieved by mixing an initially charge-neutral polymer with the anionic CNC dispersion followed by stimulus triggered by on-demand switching of cationic groups within the polymer. The resulting polycationic chains would then force the formation of ionically interacting mixtures in situ, leading to aqueous gel networks. In this case, the use of photocleavable chemical groups could be an interesting approach.[49] However, in the context of CNC, no previous literature exists to provide irradiation triggered hydrogelation.

Here, we first report mixtures of anionic CNCs and an initially neutral random methacrylate terpolymer, allowing a homogeneous aqueous mixture. The polymer contains UV-cleavable groups, thus exposing cationic groups, leading next to ionically cross-linked hydrogels. The suggested generic scheme is shown in Figure 1. In particular, the polymer was selected to involve a lower critical solution temperature (LCST) behavior, that is, the aqueous polymer chains collapse upon heating past a critical temperature. We show that depending on the thermal history and compositions, thermoreversible or irreversible gelation can be achieved.

2. EXPERIMENTAL SECTION

2.1. Materials. All solvents and reagents were purchased from Sigma-Aldrich or VWR with ≥95% purity and used as received if not stated otherwise. Azobisisobutyronitrile (AIBN) was recrystallized from diethyl ether before use and stored in the fridge. All monomers were purified by passing through a column containing aluminum oxide (activated basic) prior to polymerization. Ultrapure Milli-Q (MQ) water (18 mΩ) was used in all experiments.

2.2. Cellulose Nanocrystals (CNCs). CNCs were prepared from a Whatman grade I filter paper according to a published procedure.[51] The filter paper was first mechanically ground into a fine powder. An amount of 15.0 g of the powder was hydrolyzed with 64% sulfuric acid at 45 °C for 45 min under gentle mechanical stirring. The reaction was stopped by diluting it 10-fold with 3 L of Milli-Q H_2O. The dispersion was left to sediment for 20 h after which the clear supernatant was discarded, and the precipitate was washed by two cycles of centrifugation and redispersion in Milli-Q H_2O. The remaining CNC dispersion was further purified by dialysis against Milli-Q H_2O until the conductivity of the dialysate remained <5 μS/cm. Finally, the CNCs were filtered through a Whatman 541 filter paper and stored at 4 °C until use.

2.3. Synthesis of 2-((2-Nitrobenzyl)oxycarbonyl)aminoethyl Methacrylate (NBOCAEMA). The monomer was synthesized as previously reported.[52−54] An amount of 4.34 g (80% purity, 24.3 mmol) of 2-nitrobenzyl alcohol was dissolved in 80 mL of THF. The insoluble solids were removed via filtration after 10 min of stirring at room temperature. Four milliliters (28.3 mmol) of isocyanatoethyl methacrylate and 130 μL (220 μmol) of dibutyltin dilaurate catalyst were added, and the mixture was stirred overnight at room temperature. Subsequently, the solvent was removed in vacuum, and the residue was dissolved in dichloromethane. The dissolved product was washed with diluted hydrochloric acid twice and neutralized by washing with water. The solution was dried with calcium chloride and filtered through a column packed with aluminum oxide (activated basic). After evaporation of the solvent, the product was obtained as a yellowish white solid in 93% yield. Purity was proven by ^{1}H-NMR spectroscopy (see Figure S1).

^{1}H-NMR (300 MHz, $CDCl_3$): 7.8−7.4 ppm (m, 4H, Ar−*H*), 6.13 ppm (s, 1H, DB−*H*), 5.6 ppm (s, 1H, DB−*H*), 5.53 ppm (s, 2H, −O−CH_2−Ar) 5.19 ppm (s, 1H, −N*H*−), 4.26 ppm (t, 2H, −C(O)O−CH_2−), 3.54 ppm (quar, 2H, −CH_2−NH−), 1.95 ppm (s, 3H, −CH_3).

2.4. Synthesis of PDEGMA$_{417}$-*rnd*-POEGMA$_{109}$-*rnd*-PNBOCAEMA$_{54}$ Terpolymer. ATRP polymerization[55] was made using LCST-inducing repeating units di(ethylene glycol) methyl ether methacrylate (DEGMA) and oligo(ethylene glycol) methyl ether methacrylate (OEGMA),[56,57] as well as the photocleavable repeating units NBOCAEMA. A total of 6.05 mL (32.8 mmol) DEGMA, 4.8 mL (10.4 mmol) OEGMA (M_n = 500), 3.36 g (10.9 mmol) NBOCAEMA, 54 mg (545 μmol) copper (I) chloride, and 170 mg (1.1 mmol) 2−2′-bipyridyl were dissolved in 15 mL of absolute

https://dx.doi.org/10.1021/acs.biomac.9b01519
Biomacromolecules 2020, 21, 830−838

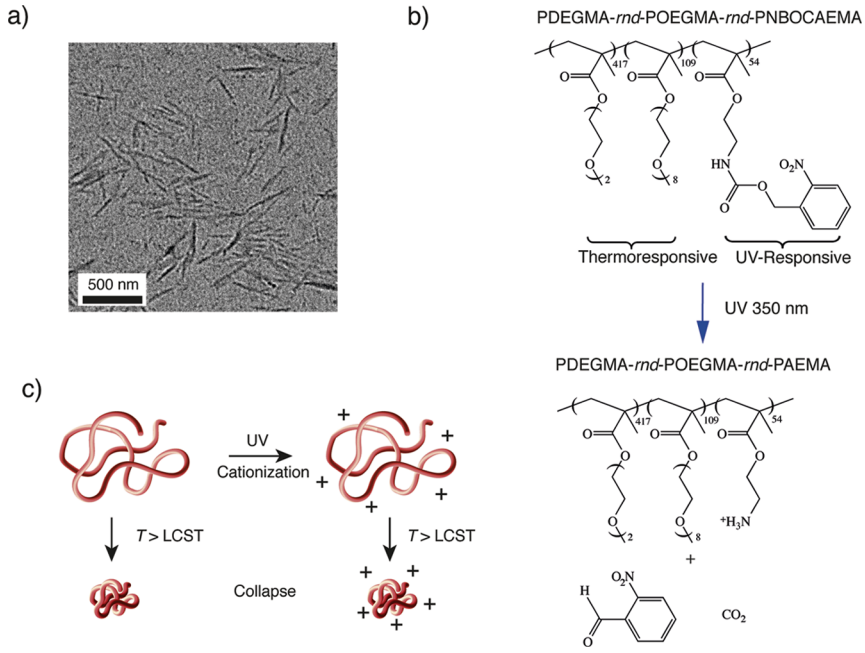

Figure 2. (a) TEM micrograph of aqueous CNCs. (b) PDEGMA$_{417}$-*rnd*-POEGMA$_{109}$-*rnd*-PNBOCAEMA$_{54}$ random terpolymer, suggesting a thermoresponsive LCST behavior in water and UV-triggerable cationization. (c) Schematics of the UV-triggerable positive polymer charging and the temperature-driven collapse and segregation from water.

ethanol. After degassing for 10 min, 80 μL (546 μmol) of ethyl 2-bromo-2-methylpropionate (EBiB) was added, and degassing was continued for 20 min. The mixture was then polymerized for 10 h at 60 °C. After cooling to room temperature, the solution was flushed with air to oxidize the copper (I) and filtered via basic aluminum oxide to remove the oxidized catalyst. The solution was then concentrated at the rotary evaporator, and the terpolymer was precipitated in cold diethyl ether twice. Drying in vacuum yielded 5.8 g (40%) of a yellow, highly viscous polymer. ^{1}H-NMR-analysis (Figure S2) in combination with SEC measurements (Figure S3) gave a composition of PDEGMA$_{417}$-*rnd*-POEGMA$_{109}$-*rnd*-PNBOCAEMA$_{54}$.

SEC (THF): $M_n \approx 160{,}000$ g·mol^{-1}, $Đ \approx 1.99$.

^{1}H-NMR (300 MHz, $CDCl_3$): 8.2−7.4 ppm (m, 4H, Ar−*H*), 6.2 ppm (s, br, 1H, −N*H*−), 5.53 ppm (s, 2H, −O−C*H*$_2$−Ar) 4.1 ppm (t, 2H, −C(O)O−C*H*$_2$−), 3.8−3.5 ppm (br, −C*H*$_2$−), 3.4 ppm (s, 3H, O−C*H*$_3$), 2.3−0.5 ppm (3H, −C*H*$_3$).

2.5. Preparation of Mixtures of CNC and PDEGMA$_{417}$-*rnd*-POEGMA$_{109}$-*rnd*-PNBOCAEMA$_{54}$. We prepared 3 vol % (total solids volume concentration) dispersions of the anionically charged CNCs (bulk density 1.6 g/mL) with the charge-neutral PDEGMA$_{417}$-*rnd*-POEGMA$_{109}$-*rnd*-PNBOCAEMA$_{54}$ (density 1.2 g/mL) in Milli-Q water. Six compositions of CNC:PDEGMA$_{417}$-*rnd*-POEGMA$_{109}$-*rnd*-PNBOCAEMA$_{54}$ were used: 4:1, 2:1, 1:1, 1:2, 1:4, and 1:8 vol:vol.

2.6. UV Irradiation. The samples were irradiated for 4 h using a Rayonet RPR-200 photochemical chamber reactor with RPR-3500A lamps (350 nm) nominally at room temperature. However, irradiation tended to warm the samples. Therefore, in order to prevent excessive warming of the solutions, the sample vials were stored in a fridge until they cooled down after every 30 min of UV irradiation.

2.7. Gelation. Samples were heated in an oven set to 60 °C. The typical heating periods were 30 min or 20 h.

2.8. Dynamic Light Scattering (DLS) and Zeta Potential (ζ). DLS and zeta potential measurements were performed with a Zetasizer nano ZS90 (Malvern Instruments). Square polystyrene cuvettes (12 mm; product no. DTS0012, Malvern Instruments) were used for DLS, and folded capillary zeta cell cuvettes (product no. DTS1070, Malvern Instruments) were used for zeta potential determination. CNC (1 mg/mL) and PDEGMA$_{417}$-*rnd*-POEGMA$_{109}$-*rnd*-PNBOCAEMA$_{54}$ dispersion in Milli-Q H_2O were used for both types of experiments, but an additional 1.0 mM of NaCl was used in the zeta potential samples. Measurements were conducted at neutral pH 7 and pH 4, which is roughly the pH for different CNC:PDEGMA$_{417}$-*rnd*-POEGMA$_{109}$-*rnd*-PNBOCAEMA$_{54}$ compositions. The reported distributions and values are the average of three measurements.

2.9. Conductometric Titration. Conductometric titration of CNCs was done according to the SCAN-CM 65:02 procedure as described earlier by using a 751 GDP Titrino (Methrom AG) conductometric titrator and Tiamo software.[58,59] Before the measurement, CNC acidic groups were protonated with HCl. Concentrated HCl was added to the CNC dispersion up to 0.1 M final concentration. The mixture was equilibrated for 15 min at 22 °C, after which it was dialyzed against MQ H_2O until the conductivity of the sample remained below 5 μS/cm to remove the excess HCl. The titration sample was prepared by adding 490 mL of degassed MQ H_2O, 0.5 mL of 0.1 M HCl, and 1.0 mL of 0.5 M NaCl to 20 mL of the protonated CNCs (c = 15.9 mg/mL). The sample was titrated against 0.1 M NaOH under constant stirring (300 rpm). NaOH was added in 20 μL increments every 30 s. The acidic sulfate half ester content of CNCs was calculated as the ratio of the amount of NaOH required to neutralize the acidic groups (in μmol) to the amount of CNCs (g).

2.10. Transmission Electron Microscopy (TEM) and Size Analysis. The CNCs were imaged with JEM-2800 (JEOL) high-resolution TEM operating at 200 kV. A 10 μL droplet of 1 mg/mL CNC dispersion was pipetted onto a plasma-cleaned carbon film grid (Electron Microscopy Sciences), incubated for 1 min and then blotted with a filter paper. The average size of the CNCs was determined from the images by using ImageJ.[60,61]

2.11. Nuclear Magnetic Resonance Spectroscopy (^{1}H-NMR). ^{1}H-NMR spectra were recorded with a Bruker Avance spectrometer operating at 300 MHz and 25 °C. Measurements were performed using deuterated chloroform ($CDCl_3$) or deuterated water (D_2O). The residual solvent peaks (7.26, 5.32, and 1.56 ppm) were used as a standard for peak calibration.

2.12. Size-Exclusion Chromatography (SEC). The molar mass was determined with a Waters Acquity APC system with Acquity APC XT 200 Å, 450 Å columns at 30 °C, and UV and RI detectors. The system was calibrated with conventional calibration using third-order

https://dx.doi.org/10.1021/acs.biomac.9b01519
Biomacromolecules 2020, 21, 830−838

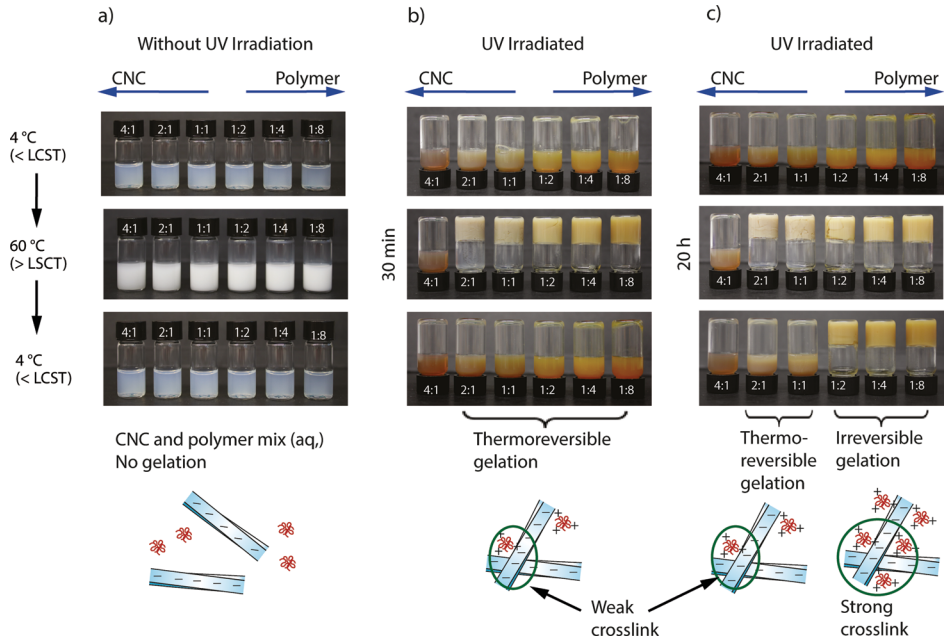

Figure 3. Sol−gel transitions illustrated by the vial inversion tests. (a) Using the charge-neutral polymer: CNC:PDEGMA$_{417}$-*rnd*-POEGMA$_{109}$-*rnd*-PNBOCAEMA$_{54}$ for 4:1−1:8 vol:vol. The neutral polymer mixes well with the anionic CNC. No gelation is observed even upon 30 min heating to 60 °C. (b) Using the cationized polymer after the UV irradiation: CNC:PDEGMA$_{417}$-*rnd*-POEGMA$_{109}$-*rnd*-PAEMA$_{54}$ for 4:1−1:8 vol:vol upon a short heating (30 min) at 60 °C. In this case, thermoreversible gelation is observed obviously as only a small extent of cross-linking is formed due to segregation driven by heating to T > LCST. (c) Cationized polymer after the UV irradiation: CNC:PDEGMA$_{417}$-*rnd*-POEGMA$_{109}$-*rnd*-PAEMA$_{54}$ for 4:1−1:8 vol:vol using a long heating (20 h) at 60 °C. The long heating at T > LCST promotes the extent of cross-linking. In this case, both thermoreversible and irreversible gelation can be observed, depending on the composition. Note that the panels (b) and (c) show only the inverted vials.

fitting and poly(methyl methacrylate) (PMMA) standards from PSS. The eluent was THF + 1 mg/L of tetra-*n*-butylammonium bromide (TBAB) running at 0.8 mL/min. The sample was dissolved into eluent with a concentration of 1 mg/mL, solvated overnight on a shaking table and filtered through a 0.45 μm Teflon (PTFE) filter into SEC vials before measurement.

2.13. Turbidimetry. Cloud points (CP) of the samples were determined with a Jasco V-750 Spectrophotometer operating at 600 nm with a Jasco CTU-100 circulating thermostat unit attached. The temperature range was set from 20 to 70 °C at a heating rate of 1 °C/min. The samples were prepared into 10 mm quartz cuvettes with a concentration of 0.5 mg/mL and measured during the same day. Due to inadequate signal in this concentration, PDEGMA$_{417}$-*rnd*-POEGMA$_{109}$-*rnd*-PAEMA$_{54}$ and composition 2:1 vol:vol were measured with a concentration of 1 mg/mL.

2.14. Oscillatory Rheology. TA Instruments AR2000 stress-controlled rheometer with a 20 mm steel plate-plate geometry and a Peltier heated plate were used for rheological characterization. The linear viscoelastic region for measurements was confirmed with strain sweeps. Measurements were performed using an oscillation frequency of 1.0 rad/s. After UV irradiation, liquid samples were pipetted on the 20 °C rheometer allowing in situ gelation during the measurements. The temperature was increased to 40 °C, and the time sweeps were measured for 30 min at a 0.3% strain amplitude during the gelation, followed by a frequency sweep and a strain sweep at 40 °C. The frequency sweeps were carried out at 0.1 Pa. Temperature ramps from 20 to 80 °C were measured with a 0.3% strain amplitude and 2 °C/min heating rate from liquid samples. Temperature ramps were acquired twice and all the other measurements in triplicate. Data is reported as average.

2.15. Scanning Electron Microscopy (SEM). Scanning electron microscopy images were imaged with a Zeiss Sigma VP scanning electron microscope with an accelerating voltage of 1.5 kV. Gel samples were frozen in liquid propane and freeze-dried. Prior to the imaging, aerogel samples were coated with 4 nm iridium coating using a Leica EM ACE600 high vacuum sputter coater.

3. RESULTS AND DISCUSSION

The materials are shown in Figure 2. The CNCs were characterized via light scattering and ζ-potential measurements as well as electron microscopy. An exemplary TEM image is shown in Figure 2a, suggesting an average CNC length of 241 ± 88 nm and a width of 17 ± 4 nm (Figure S4), indicating an aspect ratio of approximately 14. Due to the sulfuric acid hydrolysis, the surface hydroxyl groups of CNCs are partially esterified to anionic sulfate ester groups, rendering the surface negatively charged. Apparent ζ-potentials and electrophoretic mobilities were −56 mV and −4.41 μmcm/Vs, respectively, at pH 7 and −44 mV and −3.45 μmcm/Vs, respectively, at pH 4 (Figure S5), facilitating the stability of the CNCs in aqueous dispersions.[62] The sulfate content was determined by conductometric titration to be 239 μmol/g (Figure S6). To form homogeneous aqueous mixtures with CNCs, we used an initially neutral random terpolymer PDEGMA$_{417}$-*rnd*-POEGMA$_{109}$-*rnd*-PNBOCAEMA$_{54}$ consisting of photocleavable NBOCAEMA repeat units and DEGMA and OEGMA repeat units, allowing LCST behavior. The cleavage of the protected amine moieties of PNBOCAEMA was investigated via ^{1}H-NMR spectroscopy in D_2O (Figure S7). Comparing the integrals of the cleaved 2-nitrobenzyl group indicates approximately 90% cleavage upon 2 h of UV irradiation. Therefore, to ensure an efficient cleavage, an irradiation time of 4 h was subsequently used. That the polymer becomes cationic upon the UV trigger is shown in Figure S7. The thermoresponsive behavior of PDEGMA$_{417}$-*rnd*-POEGMA$_{109}$-*rnd*-PNBOCAEMA$_{54}$ was characterized via turbidimetry (Figure S8). Due to the relatively low signal, the exact value could not be obtained. However, we estimated the cloud point temperature (T_{cp}) in water to be roughly 43 °C. Zeta potential

https://dx.doi.org/10.1021/acs.biomac.9b01519
Biomacromolecules 2020, 21, 830−838

measurements of the terpolymer showed a shift from slightly negative to close to zero ζ-potential before and after UV exposure at pH 7. At pH 4, simulating the acidic environment when combining terpolymer with CNCs, we can see clear shift from negative to positive ζ-potential before and after UV exposure indicating the positive charge of PDEGMA$_{417}$-*rnd*-POEGMA$_{109}$-*rnd*-PNBOCAEMA$_{54}$ (Figure S9).

Next, aqueous mixtures of the anionic CNCs and the charge-neutral PDEGMA$_{417}$-*rnd*-POEGMA$_{109}$-*rnd*-PNBOCAEMA$_{54}$ polymers were prepared at room temperature for their relative volumetric compositions 4:1, 2:1, 1:1, 1:2, 1:4, and 1:8 vol:vol by keeping the total solid concentrations fixed at 3.0 vol %. In all mixtures, slightly opaque fluid-like dispersions were observed at 4 °C, obviously due to the colloidal nature of the CNCs. The LCST of the pure polymer was determined to be about 43 °C (Figure S8), but in the composites, the transition is shifted to lower temperatures with an increasing amount of CNCs present, as will be discussed later. Fluid-like dispersions at 4 °C are observed as the polymer is fully soluble, and the CNCs are repelling due to their negative surface charge. Importantly, the dispersions seem visually homogeneous and stable (Figure 3a). This finding supports the hypothesis to achieve a robust homogeneous mixing of the negative CNCs and neutral PDEGMA$_{417}$-*rnd*-POEGMA$_{109}$-*rnd*-PNBOCAEMA$_{54}$ in aqueous media. Note that polarized optical microscope imaging (POM) of the mixtures with crossed polarizers did not show any birefringence at any point of the processing. Heating to 60 °C (30 min) leads to a cloudy appearance (Figure 3a) as the PDEGMA$_{417}$-*rnd*-POEGMA$_{109}$-*rnd*-PNBOCAEMA$_{54}$ polymer chains collapse, as the temperature is beyond its LCST cloud point 43 °C (Figure S8). Upon recooling to 4 °C, the original translucency is recovered, indicating reversibility.

After being homogeneously mixed, UV irradiation is next applied to drive the on-demand cationization of the polymer (see Figure 2) to achieve the electrostatic complexation with the anionic CNC. Figure 3b shows the CNC:PDEGMA$_{417}$-*rnd*-POEGMA$_{109}$-*rnd*-PAEMA$_{54}$ compositions ranging from the high relative volume fraction of CNC (4:1 vol:vol) to the high relative volume fraction of the polymer (1:8 vol:vol). Slightly surprisingly, at 4 °C all compositions are stable and homogeneous dispersions (instead of flocculation[63]) or gels, and the mixtures are yellowish-brown depending on the composition, as caused by the near-UV-absorption of the released 2-nitrobenzaldehyde molecules. Furthermore, an increase of turbidity (Figure 3b,c) was observed, suggesting an increased interaction of the anionically charged CNCs and the now positively charged terpolymer PDEGMA$_{417}$-*rnd*-POEGMA$_{109}$-*rnd*-PAEMA$_{54}$. As will be later discussed in the connection of Figure 4, all studied CNC:PDEGMA$_{417}$-*rnd*-POEGMA$_{109}$-*rnd*-PAEMA$_{54}$ compositions show LCST behavior. Therefore, heating to 60 °C is expected to promote phase segregation of the DEGMA and OEGMA repeat units. Interestingly, heating to 60 °C for a short time of 30 min leads to gelation, except for the composition 4:1 vol:vol, that is, involving the smallest amount of the polymer, see Figure 3b. Cooling back to 4 °C, all compositions are again fluid. A similar procedure was repeated by keeping the CNC:PDEGMA$_{417}$-*rnd*-POEGMA$_{109}$-*rnd*-PAEMA$_{54}$ for a longer time (20 h) at 60 °C (Figure 3c). In this case, a more complex behavior was observed. At the smaller polymer fraction (4:1 vol:vol), no gelation was observed at 60 °C, as was the case also for the shorter heating. Similarly, for the compositions 2:1 and 1:1

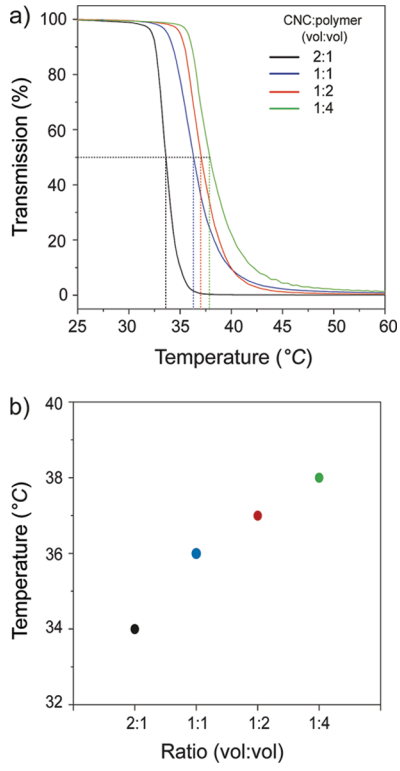

Figure 4. Turbidity measurements for CNC:PDEGMA$_{417}$-*rnd*-POEGMA$_{109}$-*rnd*-PAEMA$_{54}$ 2:1, 1:1, 1:2, and 1:4 vol:vol. (a) Turbidity data. (b) Tunability of the LCST behavior where the cloud point is shown to increase when the polymer fraction is increased.

vol:vol, thermoreversible gelation was observed, as the fluid behavior was regained upon cooling back to 4 °C. However, for the highest polymer volume fractions (1:2, 1:4, 1:8 vol:vol), the fluid behavior was not regained upon cooling to 4 °C, indicating irreversible gelation. These observations suggest time-dependent restructuring of the polymer on CNCs to form the ionic cross links.

Negative control experiments were performed similarly by using only either CNCs or polymers at different concentrations (Figures S10–S11). Therein, no gelation was observed, even upon prolonged UV exposure. One can conclude that gelation is observed when both CNCs and the polymer are present where both the phototriggered polymer cationization and heating past the LCST were needed.

Therefore, the simple vial turning experiments allow mapping the elements of the complicated phase behavior and kinetic aspects. The attractive feature is that the neutral polymer precursor allows achieving homogeneous mixtures upon mixing. After the mixing, the irradiation-switched ionic interactions do not directly lead to gelation but additionally require heating past the LCST. Whether gelation is reversible or irreversible can be controlled by the polymer volume fractions as well as by the time that the compositions are heated above the LCST. Indirectly, this suggests that the material has a memory. We tentatively suggest that these attractive properties are driven by a combination of reasons: (i) DEGMA and OEGMA repeating units within PDEGMA$_{417}$-*rnd*-POEGMA$_{109}$-*rnd*-PAEMA$_{54}$ lead to LCST-behavior of the ionic complex; (ii) heating causes polymer conformational collapse and also tendency to form local aggregates of the hydrophobic domains to form ionic cross-link sites; and

https://dx.doi.org/10.1021/acs.biomac.9b01519
Biomacromolecules 2020, 21, 830−838

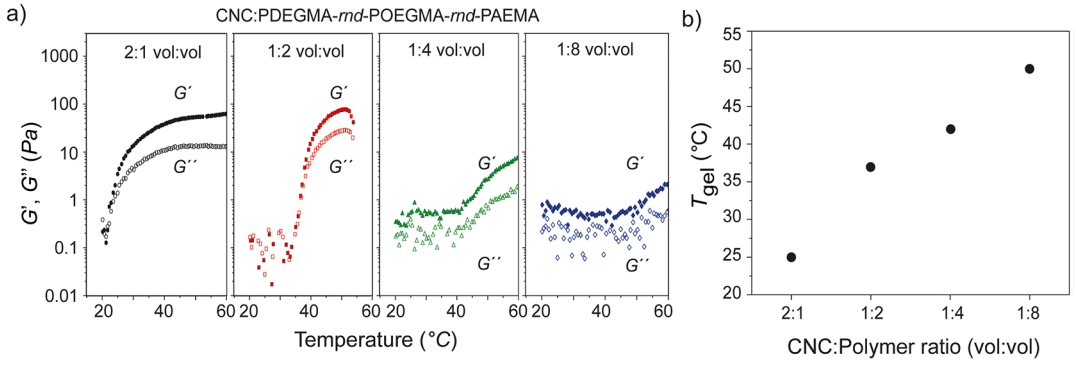

Figure 5. Dynamic rheology for the CNC:PDEGMA$_{417}$-*rnd*-POEGMA$_{109}$-*rnd*-PAEMA$_{54}$ 2:1, 1:2, 1:4, and 1:8 vol:vol compositions. (a) Temperature ramps using a 2 °C/min heating rate at 1 Hz. (b) Gelation temperatures increase when polymer volume fraction is increased.

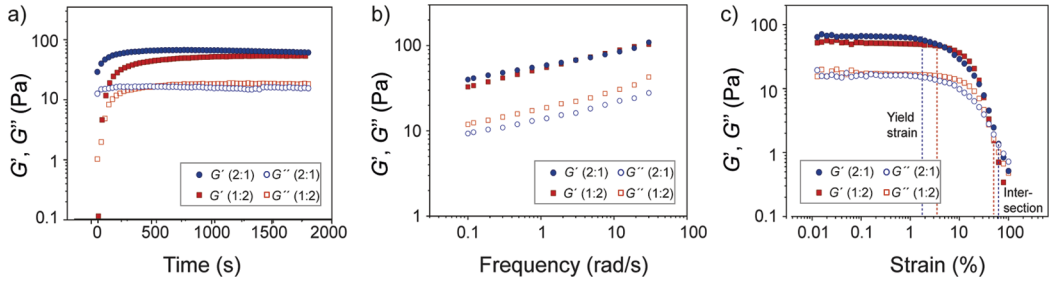

Figure 6. Oscillatory rheology of CNC:PDEGMA$_{417}$-*rnd*-POEGMA$_{109}$-*rnd*-PAEMA$_{54}$ 2:1 and 1:2 vol:vol compositions at 40 °C. (a) Time sweep showing rapid gelation and stabilization of gels following the step-wise increase of the temperature from the room temperature to 40 °C. (b) Both compositions show $G' > G''$, both only slightly depending on the frequency, as expected for gels. (c) Strain sweep showing strain-softening behavior of the gels. Dotted lines show yield strains and intersections of G' and G''.

(iii) if the polymer fraction is small, the ionic cross-link domains remain small and few, not sufficient to allow irreversible gelation, instead leading to reversible gelation. By contrast, if the polymer fraction is large, stronger ionically cross-linked networks are formed during the prolonged heating to 60 °C, leading to irreversible gelation.

Cloud points were studied via turbidity measurements using CNC:PDEGMA$_{417}$-*rnd*-POEGMA$_{109}$-*rnd*-PAEMA$_{54}$ with 2:1, 1:1, 1:2, and 1:4 vol:vol (Figure 4). They depend slightly on the CNC:polymer ratio. All CNC:PDEGMA$_{417}$-*rnd*-POEGMA$_{109}$-*rnd*-PAEMA$_{54}$ compositions showed lower cloud points than the pure polymer ($T_{cp} \approx 43$ °C) (Figure S8). The composition with the highest CNC concentration showed the lowest cloud point temperature (34 °C) and vice versa.

The effect of total solid concentration for gelation was inspected using CNC:PDEGMA$_{417}$-*rnd*-POEGMA$_{109}$-*rnd*-PAEMA$_{54}$: 2:1 vol:vol (Figure S12). Therein, the critical concentration of total solids to allow gelation upon heating was approximately 2.5% vol. Two composition ranges were selected for more detailed investigations using oscillatory rheology, that is, representing reversible gelation (2:1 and 1:1 vol:vol) and irreversible gelation (1:2 and 1:4 vol:vol) (Figure 3c) upon recooling from 60 to 4 °C (Figure 5). Temperature ramp experiments were first measured starting from 20 °C using the sweep rate 2 °C/min (Figure 5a). Gelation temperatures were estimated from the intersection of storage modulus (G') and loss modulus (G'') for the compositions 2:1 and 1:2 vol:vol where G' intersected G'' unambiguously. Because compositions 1:4 and 1:8 vol:vol did not show clear intersection of G' and G'', we roughly estimated the gelation temperature from the point where the moduli start increasing from those of the viscous fluid level (Figure 5a). Note that as the rheological measurement parameters are chosen according to the elastic gel state, the noise levels in the easily flowing fluid state turn high (Figure 5). The gelation temperatures (T_{gel}) vary between 23 and 51 °C for the different CNC:terpolymer ratios (Figure 5b), where the highest CNC fraction shows the lowest gelation temperature. This trend thus suggests the importance of the LCST and the cloud points (T_{CP}) for the gelation mechanism (Figure 4b). We also point out that especially for the composition 1:2 vol:vol, a massive shrinking of the sample volume were observed during the gelation and thus suggesting an erroneous drop in the seeming moduli values due to reduced contact of the rheometer plates upon exceeding approximately 50 °C.

Gels of PDEGMA$_{417}$-*rnd*-POEGMA$_{109}$-*rnd*-PAEMA$_{54}$ with 2:1 and 1:2 vol:vol were chosen for further rheological experiments (Figure 6, Figures S13–S14), as suggested by their different gelation behaviors (thermoreversible and irreversible gelation) in the vial inversion testing (Figure 3b,c). Frequency sweeps at 60 °C turned unreliable due excessive slip due to massive gel contraction. The slip could better be controlled at 40 °C, which was still above the gelation temperatures of both compositions. Following the step-wise temperature increase to 40 °C, a rapid gelation of both compositions is observed in time sweeps (Figure 6a) where composition 2:1 vol:vol forms a gel and stabilizes slightly faster, presumably due to its lower T_{gel}. The storage moduli of both compositions were obtained from plateau values in the end of the time sweep and were found to be approximately the same ($G' \approx 60$ Pa and $G'' \approx 15$ Pa) for both compositions. The moduli of both compositions show only a small dependency of frequency as expected for elastic gels where the moduli are ideally independent of the frequency (Figure

https://dx.doi.org/10.1021/acs.biomac.9b01519
Biomacromolecules 2020, 21, 830−838

6b). The gels behave as strain-softening materials where the stiffness decreases when strain is increasing beyond the linear viscoelastic region (LVR) (Figure 6c). Yield strain, where plastic deformation starts to occur, was slightly at a lower strain in the composition 2:1 vol:vol than in 1:2 vol:vol. Finally, the gels break down or detach from the plates almost at the same strains where G' and G'' intersect.

We postulate that the cross-linkings in the CNC:PDEGMA$_{417}$-*rnd*-POEGMA$_{109}$-*rnd*-PAEMA$_{54}$ gels are mediated by ionic interactions. To directly prove this, increasing the ionic strength is a way to increase the ionic screening and to reduce the Debye screening length. To illustrate this, Figure 7 and

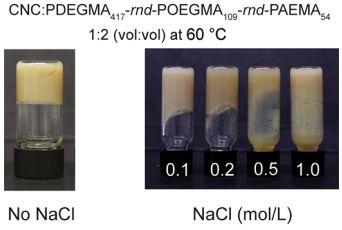

Figure 7. CNC:PDEGMA$_{417}$-*rnd*-POEGMA$_{109}$-*rnd*-PAEMA$_{54}$ 1:2 vol:vol at 60 °C with various concentrations of NaCl, showing that the gel melts upon adding NaCl.

Figure S15 show CNC:PDEGMA$_{417}$-*rnd*-POEGMA$_{109}$-*rnd*-PNBOCAEMA$_{54}$ 1:2 vol:vol gel at 60 °C, where various concentrations of NaCl have been added. Clearly, the addition of NaCl suppresses the gelation, directly showing that the gelation is driven by ionic interactions.

Finally, to study the gel network structures, TEM is not particularly suitable as it requires thin samples, and one expects that the polymer component cannot easily be resolved. Therefore, we selected SEM upon freezing in liquid propane followed by lyophilization. Cooling by liquid propane suppresses the thermally insulating Leidenfrost effect and thus leads to quick freezing to reduce aggregations.[64] SEM images of CNC:PDEGMA$_{417}$-*rnd*-POEGMA$_{109}$-*rnd*-PAEMA$_{54}$ 2:1 and 1:2 vol:vol suggest differences in their network structures. The 1:2 vol:vol network consists of thicker fibers than 2:1 vol:vol, which are probably due to the higher concentration of the polymer compared to CNCs (Figure 8a,b). However, we can still see the individual CNCs on the surface of the polymer networks (Figure 8b, inset). On the contrary, the 2:1 vol:vol network consists of a higher concentration of CNCs compared to the polymer, which can be distinctly seen in the SEM image where the network consists mostly of CNCs covered with the polymer (Figure 8c,d).

4. CONCLUSIONS

In this work, the challenge to prepare ionically cross-linked hydrogels of negatively charged CNCs and positively charged polymers is addressed by preparing first a neutral polymeric "precursor", allowing homogeneous mixing with CNCs, followed by UV-triggered in situ cationization. The polymethacrylate terpolymer poly(di(ethylene glycol) methyl ether methacrylate)-*rnd*-poly(oligo(ethylene glycol) methyl ether methacrylate)-*rnd*-poly(2-((2-nitrobenzyl)oxycarbonyl)-aminoethyl methacrylate), that is, PDEGMA$_{417}$-*rnd*-POEGMA$_{109}$-*rnd*-PNBOCAEMA$_{54}$ was designed to be bifunctional: The PNBOCAEMA repeating units are UV-triggerable to

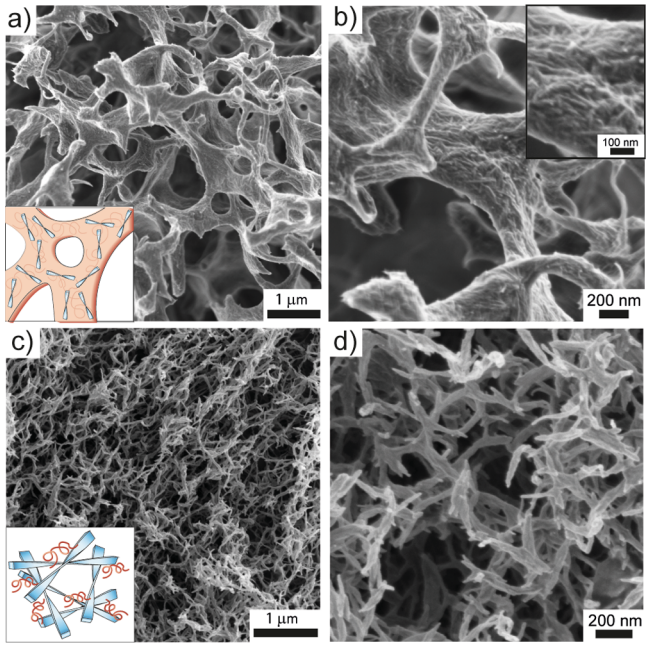

Figure 8. SEM images of freeze-dried CNC:PDEGMA$_{417}$-*rnd*-POEGMA$_{109}$-*rnd*-PAEMA$_{54}$. (a, b) 1:2 vol:vol composition. The inset shows magnification of CNCs on the surface of the terpolymer. (c, d) 2:1 vol:vol composition.

provide cationic AEMAs upon cleaving of the 2-nitrobenzaldehyde group and thus allowing ionic binding to the anionic CNCs. The DEGMA and OEGMA functionalities lead to the LCST behavior of the ionic complexes, which turns relevant to drive gelation. A range of CNC:polymer volume fractions from 2:1 to 1:8 vol:vol was explored. The cloud points 34−38 °C were determined by turbidimetry and gelling temperatures 23−51 °C by rheology. If the fraction of the polymer is sufficiently large, gelation is observed at 60 °C, that is, passing the cloud point of the complex. The ionic nature of the interaction is shown by adding NaCl, which screens the ionic interactions, thus leading to the gel melting. The gelation involves kinetic aspects combined with the compositions, as thermoreversible gelation is observed if the heating at 60 °C is short (30 min), whereas irreversible gelation results for long heating (20 h) at 60 °C. This indicates slow formation of the LCST-driven ionic cross-linkings between the CNCs. In conclusion, the concept can be generalized to prepare other ionically self-assembled systems, for example, using clay-polymer self-assemblies or interpolyelectrolyte complexes.

■ ASSOCIATED CONTENT

Supporting Information

The Supporting Information is available free of charge at https://pubs.acs.org/doi/10.1021/acs.biomac.9b01519.

DLS: zeta-potential and electrophoretic mobility analysis of the CNCs and polymer, conductometric titration and size analysis of CNCs, ^{1}H-NMR analyses of the synthesized monomer and polymer, SEC analysis of the polymer, polymer and CNC:polymer cloud point analysis, and additional rheological data (PDF)

https://dx.doi.org/10.1021/acs.biomac.9b01519
Biomacromolecules 2020, 21, 830−838

AUTHOR INFORMATION

Corresponding Author

Olli Ikkala − *Department of Applied Physics, Aalto University School of Science, Espoo FI-00076, Finland;* orcid.org/0000-0002-0470-1889; Email: olli.ikkala@aalto.fi

Authors

Christoph Hörenz − *Department of Applied Physics, Aalto University School of Science, Espoo FI-00076, Finland*

Kia Bertula − *Department of Applied Physics, Aalto University School of Science, Espoo FI-00076, Finland;* orcid.org/0000-0002-7134-3591

Tony Tiainen − *Department of Chemistry, University of Helsinki, Helsinki FI-00014 HU, Finland*

Sami Hietala − *Department of Chemistry, University of Helsinki, Helsinki FI-00014 HU, Finland*

Ville Hynninen − *Department of Applied Physics, Aalto University School of Science, Espoo FI-00076, Finland*

Complete contact information is available at: https://pubs.acs.org/10.1021/acs.biomac.9b01519

Funding

This work was supported by the Academy of Finland through the Center of Excellence of Molecular Engineering of Biosynthetic Hybrid Materials (HYBER; decision no. 272361), by Business Finland (Grant no: 2489/31/2017), and the FinnCERES Flagship project.

Notes

The authors declare no competing financial interest.

ACKNOWLEDGMENTS

This work made use of the Aalto University Nanomicroscopy Center (Aalto-NMC) premises. The authors acknowledge Joona Kontinen from the Department of Chemistry at the University of Helsinki for helping with SEC measurements. Dr. Nonappa is acknowledged for discussions.

REFERENCES

(1) Klemm, D.; Kramer, F.; Moritz, S.; Lindström, T.; Ankerfors, M.; Gray, D.; Dorris, A. Nanocelluloses: A New Family of Nature-Based Materials. *Angew. Chem., Int. Ed.* **2011**, *50*, 5438−5466.

(2) Kontturi, E.; Laaksonen, P.; Linder, M. B.; Nonappa; Gröschel, A. H.; Rojas, O. J.; Ikkala, O. Advanced materials through assembly of nanocelluloses. *Adv. Mater.* **2018**, *30*, 1703779.

(3) Habibi, Y.; Lucia, L. A.; Rojas, O. J. Cellulose Nanocrystals: Chemistry, Self-assembly, and Applications. *Chem. Rev.* **2010**, *110*, 3479−3500.

(4) *Polymeric and Self Assembled Hydrogels: From Fundamental Understanding to Applications*; Loh, X. J.; Scherman, O.A., Eds.; Royal Society of Chemistry: U.K., 2013.

(5) Pääkkö, M.; Ankerfors, M.; Kosonen, H.; Nykänen, A.; Ahola, S.; Österberg, M.; Ruokolainen, J.; Laine, J.; Larsson, P. T.; Ikkala, O.; Lindström, T. Enzymatic Hydrolysis Combined with Mechanical Shearing and High-Pressure Homogenization for Nanoscale Cellulose Fibrils and Strong Gels. *Biomacromolecules* **2007**, *8*, 1934−1941.

(6) Saito, T.; Uematsu, T.; Kimura, S.; Enomae, T.; Isogai, A. Self-aligned integration of native cellulose nanofibrils towards producing diverse bulk materials. *Soft Matter* **2011**, *7*, 8804−8809.

(7) Choi, Y.; Simonsen, J. Cellulose nanocrystal-filled carboxymethyl cellulose nanocomposites. *J. Nanosci. Nanotech.* **2006**, *6*, 633−639.

(8) Zhou, C.; Wu, Q.; Zhang, Q. Dynamic rheology studies of in situ polymerization process of polyacrylamide-cellulose nanocrystal composite hydrogels. *Colloid Polym. Sci.* **2011**, *289*, 247−255.

(9) Abitbol, T.; Johnstone, T.; Quinn, T. M.; Gray, D. G. Reinforcement with cellulose nanocrystals of poly(vinyl alcohol) hydrogels prepared by cyclic freezing and thawing. *Soft Matter* **2011**, *7*, 2373−2379.

(10) Ureña-Benavides, E. E.; Ao, G.; Davis, V. A.; Kitchens, C. L. Rheology and phase behavior of lyotropic cellulose nanocrystal suspensions. *Macromolecules* **2011**, *44*, 8990−8998.

(11) Way, A. E.; Hsu, L.; Shanmuganathan, K.; Weder, C.; Rowan, S. J. pH-Responsive Cellulose Nanocrystal Gels and Nanocomposites. *ACS Macro Lett.* **2012**, *1*, 1001−1006.

(12) Yang, J.; Han, C.-R.; Duan, J.-F.; Ma, M.-G.; Zhang, X.-M.; Xu, F.; Sun, R.-C.; Xie, X.-M. Studies on the properties and formation mechanism of flexible nanocomposite hydrogels from cellulose nanocrystals and poly(acrylic acid). *J. Mater. Chem.* **2012**, *22*, 22467−22480.

(13) Yang, J.; Han, C.-R.; Duan, J.-F.; Xu, F.; Sun, R.-C. Mechanical and Viscoelastic Properties of Cellulose Nanocrystals Reinforced Poly(ethylene glycol) Nanocomposite Hydrogels. *ACS Appl. Mater. Interfaces* **2013**, *5*, 3199−3207.

(14) Kan, K. H. M.; Li, J.; Wijesekera, K.; Cranston, E. D. Polymer-Grafted Cellulose Nanocrystals as pH-Responsive Reversible Flocculants. *Biomacromolecules* **2013**, *14*, 3130−3139.

(15) Haghpanah, J. S.; Tu, R.; Da Silva, S.; Yan, D.; Mueller, S.; Weder, C.; Foster, E. J.; Sacui, I.; Gilman, J. W.; Montclare, J. K. Bionanocomposites: Differential Effects of Cellulose Nanocrystals on Protein Diblock Copolymers. *Biomacromolecules* **2013**, *14*, 4360−4367.

(16) Hu, Z.; Cranston, E. D.; Ng, R.; Pelton, R. Tuning Cellulose Nanocrystal Gelation with Polysaccharides and Surfactants. *Langmuir* **2014**, *30*, 2684−2692.

(17) McKee, J. R.; Hietala, S.; Seitsonen, J.; Laine, J.; Kontturi, E.; Ikkala, O. Thermoresponsive Nanocellulose Hydrogels with Tunable Mechanical Properties. *ACS Macro Lett.* **2014**, *3*, 266−270.

(18) Yang, D.; Peng, X.; Zhong, L.; Cao, X.; Chen, W.; Wang, S.; Liu, C.; Sun, R. Fabrication of a highly elastic nanocomposite hydrogel by surface modification of cellulose nanocrystals. *RSC Adv.* **2015**, *5*, 13878−13885.

(19) Chau, M.; Sriskandha, S. E.; Pichugin, D.; Thérien-Aubin, H.; Nykypanchuk, D.; Chauve, G.; Méthot, M.; Bouchard, J.; Gang, O.; Kumacheva, E. Ion-Mediated Gelation of Aqueous Suspensions of Cellulose Nanocrystals. *Biomacromolecules* **2015**, *16*, 2455−2462.

(20) Domingues, R. M. A.; Silva, M.; Gershovich, P.; Betta, S.; Babo, P.; Caridade, S. G.; Mano, J. F.; Motta, A.; Reis, R. L.; Gomes, M. E. Development of injectable hyaluronic acid/cellulose nanocrystals bionanocomposite hydrogels for tissue engineering applications. *Bioconjugate Chem.* **2015**, *26*, 1571−1581.

(21) Wang, H.-D.; Jessop, P. G.; Bouchard, J.; Champagne, P.; Cunningham, M. F. Cellulose nanocrystals with CO_2-switchable aggregation and redispersion properties. *Cellulose* **2015**, *22*, 3105−3116.

(22) Larsson, E.; Boujemaoui, A.; Malmström, E.; Carlmark, A. Thermoresponsive cryogels reinforced with cellulose nanocrystals. *RSC Adv.* **2015**, *5*, 77643−77650.

(23) Azzam, F.; Siqueira, E.; Fort, S.; Hassaini, R.; Pignon, F.; Travelet, C.; Putaux, J.-L.; Jean, B. Tunable Aggregation and Gelation of Thermoresponsive Suspensions of Polymer-Grafted Cellulose Nanocrystals. *Biomacromolecules* **2016**, *17*, 2112−2119.

(24) Huang, L.; Ye, Z.; Berry, R. Modification of Cellulose Nanocrystals with Quaternary Ammonium-Containing Hyperbranched Polyethylene Ionomers by Ionic Assembly. *ACS Sustainable Chem. Eng.* **2016**, *4*, 4937−4950.

(25) Lewis, L.; Derakhshandeh, M.; Hatzikiriakos, S. G.; Hamad, W. Y.; MacLachlan, M. J. Hydrothermal Gelation of Aqueous Cellulose Nanocrystal Suspensions. *Biomacromolecules* **2016**, *17*, 2747−2754.

(26) Peddireddy, K. R.; Capron, I.; Nicolai, T.; Benyahia, L. Gelation Kinetics and Network Structure of Cellulose Nanocrystals in Aqueous Solution. *Biomacromolecules* **2016**, *17*, 3298−3304.

(27) Hu, Z.; Xu, R.; Cranston, E. D.; Pelton, R. H. Stable Aqueous Foams from Cellulose Nanocrystals and Methyl Cellulose. *Biomacromolecules* **2016**, *17*, 4095−4099.

(28) Zhang, T.; Zuo, T.; Hu, D.; Chang, C. Dual Physically Cross-Linked Nanocomposite Hydrogels Reinforced by Tunicate Cellulose Nanocrystals with High Toughness and Good Self-Recoverability. *Appl. Mater. Interfaces* **2017**, *9*, 24230−24237.
(29) Gray, D. G. Order and gelation of cellulose nanocrystal suspensions: an overview of some issues. *Philos. Trans. R. Soc., A* **2018**, *376*, 20170038.
(30) Oechsle, A.-L.; Lewis, L.; Hamad, W. Y.; Hatzikiriakos, S. G.; MacLachlan, M. J. CO_2-Switchable Cellulose Nanocrystal Hydrogels. *Chem. Mater.* **2018**, *30*, 376−385.
(31) Hynninen, V.; Hietala, S.; McKee, J. R.; Murtomäki, L.; Rojas, O. J.; Ikkala, O.; Nonappa. Inverse Thermoreversible Mechanical Stiffening and Birefringence in a Methylcellulose/Cellulose Nanocrystal Hydrogel. *Biomacromolecules* **2018**, *19*, 2795−2804.
(32) Nigmatullin, R.; Harniman, R.; Gabrielli, V.; Muñoz-García, J. C.; Khimyak, Y. Z.; Angulo, J.; Eichhorn, S. J. Mechanically robust gels formed from hydrophobized cellulose nanocrystals. *ACS Appl. Mater. Interfaces* **2018**, *10*, 19318−19322.
(33) Gicquel, E.; Martin, C.; Gauthier, Q.; Engström, J.; Abbattista, C.; Carlmark, A.; Cranston, E. D.; Jean, B.; Bras, J. Tailoring Rheological Properties of Thermoresponsive Hydrogels through Block Copolymer Adsorption to Cellulose Nanocrystals. *Biomacromolecules* **2019**, *20*, 2545−2556.
(34) Shao, C.; Meng, L.; Wang, M.; Cui, C.; Wang, B.; Han, C.-R.; Xu, F.; Yang, J. Mimicking Dynamic Adhesiveness and Strain-Stiffening Behavior of Biological Tissues in Tough and Self-Healable Cellulose Nanocomposite Hydrogels. *ACS Appl. Mater. Interfaces* **2019**, *11*, 5885−5895.
(35) Lewis, L.; Hatzikiriakos, S. G.; Hamad, W. Y.; MacLachlan, M. J. Freeze-Thaw Gelation of Cellulose Nanocrystals. *ACS Macro Lett.* **2019**, *8*, 486−491.
(36) Faul, C. F. J. Ionic Self-Assembly for Functional Hierarchical Nanostructured Materials. *Acc. Chem. Res.* **2014**, *47*, 3428−3438.
(37) Pergushov, D. V.; Müller, A. H. E.; Schacher, F. H. Micellar interpolyelectrolyte complexes. *Chem. Soc. Rev.* **2012**, *41*, 6888−6901.
(38) Kostiainen, M. A.; Hiekkataipale, P.; Laiho, A.; Lemieux, V.; Seitsonen, J.; Ruokolainen, J.; Ceci, P. Electrostatic assembly of binary nanoparticle superlattices using protein cages. *Nat. Nanotechnol.* **2013**, *8*, 52−56.
(39) Löbling, T. I.; Haataja, J. S.; Synatschke, C. V.; Schacher, F. H.; Müller, M.; Hanisch, A.; Gröschel, A. H.; Müller, A. H. E. Hidden Structural Features of Multicompartment Micelles Revealed by Cryogenic Transmission Electron Tomography. *ACS Nano* **2014**, *8*, 11330−11340.
(40) Sun, H.; Miao, L.; Li, J.; Fu, S.; An, G.; Si, C.; Dong, Z.; Luo, Q.; Yu, S.; Xu, J.; Liu, J. Self-Assembly of Cricoid Proteins Induced by "Soft Nanoparticles": An Approach To Design Multienzyme-Cooperative Antioxidative Systems. *ACS Nano* **2015**, *9*, 5461−5469.
(41) Das, B. P.; Tsianou, M. From polyelectrolyte complexes to polyelectrolyte multilayers: Electrostatic assembly, nanostructure, dynamics, and functional properties. *Adv. Colloid Interface Sci.* **2017**, *244*, 71−89.
(42) Malho, J.-M.; Morits, M.; Löbling, T. I.; Nonappa; Majoinen, J.; Schacher, F. H.; Ikkala, O.; Gröschel, A. H. Rod-Like Nanoparticles with Striped and Helical Topography. *ACS Macro Lett.* **2016**, *5*, 1185−1190.
(43) Nuttelman, C. R.; Rice, M. A.; Rydholm, A. E.; Salinas, C. N.; Shah, D. N.; Anseth, K. S. Macromolecular monomers for the synthesis of hydrogel niches and their application in cell encapsulation and tissue engineering. *Prog. Polym. Sci.* **2008**, *33*, 167−179.
(44) Raeburn, J.; McDonald, T. O.; Adams, D. J. Dipeptide hydrogelation triggered via ultraviolet light. *Chem. Commun.* **2012**, *48*, 9355−9357.
(45) Torgersen, J.; Qin, X.-H.; Li, Z.; Ovsianikov, A.; Liska, R.; Stampfl, J. Hydrogels for Two-Photon Polymerization: A Toolbox for Mimicking the Extracellular Matrix. *Adv. Funct. Mater.* **2013**, *23*, 4542−4554.
(46) Frkanec, L.; Zinic, M. Chiral bis(amino acid)- and bis(amino alcohol)-oxalamidegelators. Gelation properties, self-assembly motifs and chirality effects. *Chem. Commun.* **2010**, *46*, 522−537.
(47) Yang, Y.; Zhang, J.; Liu, Z.; Lin, Q.; Liu, X.; Bao, C.; Wang, Y.; Zhu, L. Tissue-Integratable and Biocompatible Photogelation by the Imine Crosslinking Reaction. *Adv. Mater.* **2016**, *28*, 2724−2730.
(48) Tung, S.-T.; Cheng, H.-T.; Inthasot, A.; Hsueh, F.-C.; Gu, T.-J.; Yan, P.-C.; Lai, C.-C.; Chiu, S.-H. Interlocked photo-degradable macrocycles allow one-off photo-triggerable gelation of organo- and hydrogelators. *Chem. Eur. J.* **2018**, *24*, 1522−1527.
(49) Zhao, H.; Sterner, E. S.; Coughlin, E. B.; Theato, P. o-Nitrobenzyl Alcohol Derivatives: Opportunities in Polymer and Materials Science. *Macromolecules* **2012**, *45*, 1723−1736.
(50) Zhao, Z.; Shklyaev, O. E.; Nili, A.; Mohamed, M. N. A.; Kubicki, J. D.; Crespi, V. H.; Zhong, L. Cellulose Microfibril Twist, Mechanics, and Implication for Cellulose Biosynthesis. *J. Phys. Chem. A* **2013**, *117*, 2580−2589.
(51) Edgar, C. D.; Gray, D. G. Smooth Model Cellulose I Surfaces from Nanocrystal Suspensions. *Cellulose* **2003**, *10*, 299−306.
(52) Wang, X.; Liu, G.; Hu, J.; Zhang, G.; Liu, S. Concurrent Block Copolymer Polymersome Stabilization and Bilayer Permeabilization by Stimuli-Regulated "Traceless" Crosslinking. *Angew. Chem., Int. Ed.* **2014**, *53*, 3138−3142.
(53) Yao, C.; Wang, X.; Liu, G.; Hu, J.; Liu, S. Distinct Morphological Transitions of Photoreactive and Thermoresponsive Vesicles for Controlled Release and Nanoreactors. *Macromolecules* **2016**, *49*, 8282−8295.
(54) Zhu, K.; Liu, G.; Zhang, G.; Hu, J.; Liu, S. Engineering Cross-Linkable Plasmonic Vesicles for Synergistic Chemo-Photothermal Therapy Using Orthogonal Light Irradiation. *Macromolecules* **2018**, *51*, 8530−8538.
(55) Matyjaszewski, K. Advanced Materials by Atom Transfer Radical Polymerization. *Adv. Mater.* **2018**, *30*, 1706441.
(56) Lutz, J.-F.; Hoth, A. Preparation of Ideal PEG Analogues with a Tunable Thermosensitivity by Controlled Radical Copolymerization of 2-(2-Methoxyethoxy)ethyl Methacrylate and Oligo(ethylene glycol) Methacrylate. *Macromolecules* **2006**, *39*, 893−896.
(57) Porsch, C.; Hansson, S.; Nordgren, N.; Malmström, E. Thermo-responsive cellulose-based architectures: tailoring LCST using poly(ethylene glycol) methacrylates. *Polym. Chem.* **2011**, *2*, 1114−1123.
(58) Abitbol, T.; Kloser, E.; Gray, D. G. Estimation of the surface sulfur content of cellulose nanocrystals prepared by sulfuric acid hydrolysis. *Cellulose* **2013**, *20*, 785−794.
(59) Lokanathan, A. R.; Uddin, K. M. A.; Rojas, O. J.; Laine, J. Cellulose nanocrystal-mediated synthesis of silver nanoparticles: role of sulfate groups in nucleation phenomena. *Biomacromolecules* **2014**, *15*, 373−379.
(60) Schindelin, J.; Arganda-Carreras, I.; Frise, E.; Kaynig, V.; Longair, M.; Pietzsch, T.; Preibisch, S.; Rueden, C.; Saalfeld, S.; Schmid, B.; Tinevez, J. Y.; White, D. J.; Hartenstein, V.; Eliceiri, K.; Tomancak, P.; Cardona, A. Fiji: An Open-Source Platform for Biological-Image Analysis. *Nat. Methods* **2012**, *9*, 676−682.
(61) Schneider, C. A.; Rasband, W. S.; Eliceiri, K. W. NIH Image to ImageJ: 25 Years of Image Analysis. *Nat. Methods* **2012**, *9*, 671−675.
(62) Lin, K.-H.; Hu, D.; Sugimoto, T.; Chang, F.-C.; Kobayashi, M.; Enomae, T. An Analysis on the Electrophoretic Mobility of Cellulose Nanocrystals as Thin Cylinders: Relaxation and End Effect. *RSC Adv.* **2019**, *9*, 34032−34038.
(63) Ye, L.; Miao, C.; Brook, M. A.; Pelton, R. Photoflocculation of TiO_2 Microgel Mixed Suspensions. *Langmuir* **2008**, *24*, 9341−9343.
(64) Korhonen, J. T.; Hiekkataipale, P.; Malm, J.; Karppinen, M.; Ikkala, O.; Ras, R. H. A. Inorganic Hollow Nanotube Aerogels by Atomic Layer Deposition onto Native Nanocellulose Templates. *ACS Nano* **2011**, *5*, 1967−1974.

https://dx.doi.org/10.1021/acs.biomac.9b01519
Biomacromolecules 2020, 21, 830−838